Lawrence Berkeley National Laboratory
LBL Publications

Title
Ultrashort XUV pulse absorption spectroscopy of partially oxidized cobalt nanoparticles

Permalink
https://escholarship.org/uc/item/8gn9j7j4

Journal
Journal of Applied Physics, 127(18)

ISSN
0021-8979

Authors
Schiffmann, Alexander
Toulson, Benjamin W
Knez, Daniel
et al.

Publication Date
2020-05-14

DOI
10.1063/5.0004582

Peer reviewed

eScholarship.org Powered by the California Digital Library
University of California

Ultrashort XUV pulse absorption spectroscopy of partially oxidized cobalt nanoparticles

Alexander Schiffmann,[1] Benjamin W. Toulson,[2] Daniel Knez,[3] Roman Messner,[1] Martin Schnedlitz,[1] Maximilian Lasserus,[1] Ferdinand Hofer,[3] Wolfgang E. Ernst,[1] Oliver Gessner,[2] and Florian Lackner[1,a)]

AFFILIATIONS

[1]Institute of Experimental Physics, Graz University of Technology, Petersgasse 16, 8010 Graz, Austria
[2]Chemical Sciences Division, Lawrence Berkeley National Laboratory, Berkeley, California 94720, USA
[3]Institute of Electron Microscopy and Nanoanalysis and Graz Centre for Electron Microscopy, Graz University of Technology, Steyrergasse 17, 8010 Graz, Austria

[a)]**Author to whom correspondence should be addressed:** florian.lackner@tugraz.at

ABSTRACT

High-order harmonic generation (HHG) based transient extreme ultraviolet (XUV) absorption spectroscopy is an emerging technique to trace photoinduced charge carrier dynamics in condensed phase materials with femtosecond and even attosecond temporal resolution and elemental specificity. However, its application to nanoparticulate samples that are relevant, for example, for novel photocatalytic light harvesting concepts, has been limited. This is in part due to the challenge to produce residual-free samples on ultrathin, XUV-transparent substrates as well as a widespread understanding that sparsely distributed nanoparticles do not provide sufficient contrast for XUV absorption measurements. Here, we present static XUV absorption spectra of partially oxidized Co nanowire-structures with diameters of approximately 4.5 nm and lengths between 10 and 40 nm, recorded with an ultrashort pulse HHG light source. Nanoparticles are synthesized by the agglomeration of Co atoms inside superfluid helium droplets, followed by surface deposition and oxidation in ambient air. The method is uniquely suited for residual-free synthesis of transition metal nanowires and their deposition on ultrathin substrates. Analysis by high-resolution transmission electron microscopy reveals the formation of CoO nanowires with regions of unoxidized Co in their interior. The nanoparticle samples are investigated in an HHG-driven ultrafast XUV absorption setup. Despite the low surface coverage of only 23%, the recorded spectrum exhibits a distinct absorption feature at the Co $M_{2,3}$(2p) edge near 60 eV with a peak height of about 40 mOD. The results support the feasibility of table-top ultrafast transient XUV absorption studies of photoinduced dynamics in transition metal oxide nanoparticles with sub-monolayer surface coverage.

I. INTRODUCTION

Small nanoparticles possess interesting properties that are very different from their macroscopic bulk counterparts owing to the increased surface-to-volume ratio and quantum confinement effects, which emerge when approaching the 10 nm size regime.[1] In particular, metal and transition metal nanoparticles consisting of earth-abundant materials bear great potential for photocatalytic and photovoltaic devices, providing a route toward a greener and more sustainable energy infrastructure.[2,3] The underlying physical and chemical processes are driven by charge carrier dynamics proceeding on extremely fast time scales, making it challenging to disentangle them by conventional, time-averaged methods. Here, we demonstrate that ultrafast extreme ultraviolet (XUV) absorption spectroscopy may be used for element-specific probing of partially oxidized Co nanowires. The nanoparticles are produced by quantum-vortex enabled synthesis in superfluid helium nanodroplets and deposited on ultrathin substrates with sub-monolayer coverage. The results indicate that in future experiments, transient XUV absorption spectroscopy can potentially be used to study ultrafast charge carrier dynamics[4–6] in metal/metal oxide nanoparticles with a temporal resolution in the attosecond regime.

The synthesis of CoO nanoparticle catalysts[7] typically involves solvents and surfactants.[8,9] Spherical particles may also be produced

using sputtering techniques[10] or laser ablation.[7] Helium droplet assisted nanoparticle synthesis[11,12] provides a means for the residual-free production of nanowire samples, which are particularly well suited for investigation by ultrahigh vacuum techniques such as XUV absorption spectroscopy. In this method, superfluid helium droplets pick up gas-phase Co atoms,[13,14] which preferentially agglomerate along the cores of quantum vortices.[15–17] The subsequent deposition on the substrate is cushioned by the evaporating helium,[18] resulting in very pure particles as no solvents or surfactants are involved in either the synthesis or the deposition. The accessible size regime of the formed nanoparticles ranges from small spherical clusters with diameters below 5 nm to elongated wires up to a few 100 nm in length,[11,19–21] depending on the doping rate and droplet size.[22] The stability of such nanowire-structures is governed by surface diffusion processes.[23,24] Once exposed to air, deposited transition metal particles can undergo oxidation.[25,26] For Co nanoparticles, it has been shown that an initial CoO shell layer (<1 nm) is formed rapidly around a metallic Co core; the shell thickness increases as the oxidation process proceeds on a time scale of several hours.[27,28]

We synthesize nanowires formed by helium nanodroplet deposition of metallic Co particles on 10 nm thick Si_3N_4 substrates and their subsequent exposure to ambient air. The method is ideal for the decoration of fragile, ultrathin substrates due to the soft landing process[29] and generates new possibilities for ultrafast XUV and x-ray studies of nanostructured materials. The samples are characterized by high-resolution transmission electron microscopy (HR-TEM) and energy-dispersive x-ray spectroscopy (EDXS). Diffractograms obtained from HR-TEM images allow for an analysis of the sample composition and oxidization state.

High-order harmonic generation (HHG) based techniques are well established for studying ultrafast dynamics in atoms and molecules in the gas-phase, liquids, and solids using transient reflection, absorption, or photoelectron spectroscopy.[30,31] Small nanoparticles, however, have only very recently been probed with HHG based methods employing photoelectron spectroscopy[32] but have so far not been studied in absorption. We present a first investigation of nanoparticles with sub-monolayer surface coverage using HHG based static XUV absorption spectroscopy. The results support the feasibility of future experiments to study photoinduced dynamics in metal oxide nanoparticles with femto- or attosecond temporal resolution.[4–6]

II. EXPERIMENTAL METHODS

A. Nanoparticle synthesis

Cobalt nanoparticles are formed by synthesis in helium nanodroplets, details of the employed apparatus can be found in Ref 33. In brief, high purity helium gas (99.9999%) is expanded under high pressure (20 bar) through a 5 μm nozzle into vacuum. At a nozzle temperature of 5.4 K, this leads to the generation of helium droplets consisting, on average, of $\sim 1.7 \times 10^{10}$ He atoms, corresponding to a radius of ~570 nm.[34] Subsequently, the He droplets enter a pickup chamber where they pass an oven assembly containing a resistively heated Al_2O_3 basket (estimated temperature: ~1300 °C) filled with metallic Co. After pickup of Co atoms by the droplets, metal nanoparticles are formed through collisions of Co atoms inside the doped, cold (~0.4 K) helium environment.[35] Rotation of the nanodroplets leads to the emergence of quantum vortices,[17] which attract dopant atoms through hydrodynamic forces and enhance agglomeration along the vortex cores.[15,16,22] The resulting elongated metal particles[19–21] are deposited on substrates by placing either a 0.5×0.5 mm^2, 10 nm thick Si_3N_4 substrate (Norcada NT050Z) or an amorphous carbon grid into the doped droplet beam.

The Si_3N_4 substrates are used for the XUV absorption experiments whereas carbon grids are employed to characterize the particles by transmission electron microscopy (TEM). Note that even though the carbon grids are thinner (~3 nm) than the Si_3N_4 substrates, they cannot be used for XUV absorption spectroscopy as the ultrathin regions are confined to small areas supported by a thick mesh grid structure. However, carbon grids allow for better contrast in the TEM images, considering the small diameters of the particles and the relatively light elements involved.

The Co vapor pressure is adjusted for maximum pickup and deposition rate, which is measured with a quartz crystal microbalance inserted into the He droplet beam before and after deposition. The total deposition time per sample was 120 min. Both samples are prepared under the same synthesis and deposition conditions. After deposition, for both substrates, the nanoparticles are exposed to ambient air for about 1 h, leading to partial oxidation (see below). In principle, the degree of oxidation can be controlled by the exposure time. The Si_3N_4 sample was stored in Ar during transport to the XUV setup.

B. Transmission electron microscopy

A Tecnai F20 (FEI Company) high-resolution transmission electron microscope (HR-TEM) is used to study the structure and chemical composition of the deposited nanoparticles. Measurements are performed at an acceleration voltage of 200 kV. The microscope is equipped with a high-resolution Gatan imaging filter including an UltraScan CCD camera (2048×2048 pixels^2), which is used for the acquisition of the micrographs. For energy-dispersive x-ray spectroscopy (EDXS), an EDAX Sapphire Si(Li) detector is used.

C. XUV absorption spectroscopy setup

The ultrafast XUV setup has been described elsewhere.[36,37] HHG is performed by focusing 50% of the output of a 785 nm, 3.3 mJ, 3 kHz, 40 fs full-width-at-half-maximum (FWHM) Ti:sapphire laser system into a semi-infinite gas cell filled with about 150 Torr of neon. A quasi-continuous XUV spectrum consisting of overlapping harmonics is generated, spanning from 48 to 72 eV photon energy. Harmonics beyond 72 eV and the remaining light from the IR driving laser are suppressed by Al filters. The XUV beam is focused to a 1/e diameter of about (23 ± 5) μm (determined by a knife-edge scan) at the sample using a toroidal mirror. After passing through the sample, the XUV beam is spectrally dispersed by a concave spherical variable-line-spacing grating. The XUV spectrum is detected by an x-ray CCD camera.

To record XUV absorption spectra of the nanoparticles, the sample is repeatedly driven in and out of the XUV beam, recording reference spectra (I_{ref}) without the sample and spectra with the sample inserted (I_{sig}) for 30 s each. The recorded spectra are given in units of optical density: $OD = \log(I_{ref}/I_{sig})$. Data presented here

correspond to an average over six individually recorded spectra, i.e., a total data acquisition time of 6 min.

III. RESULTS AND DISCUSSION

Representative TEM images of the fabricated cobalt nanoparticles are shown in Fig. 1, panel (a) and (b), at two different scales. At the chosen synthesis conditions, the obtained nanostructures are comprised of short nanowires, some of which agglomerated to larger structures or lie on top of each other while some particles remain separated. After deposition, the nanoparticles can oxidize during exposure to air for about 1 h.

Images recorded at different positions on the TEM grid are analyzed with the FIJI software package,[38] revealing an average surface coverage of about $(23 \pm 6)\%$ (uncertainties refer to 95% confidence intervals). The mean diameter of the nanowire-like particles is estimated from the images to (4.5 ± 1.5) nm and the length between 10 and 40 nm. A more detailed analysis of particle diameters and lengths can be found in the supplementary material.

Energy-dispersive x-ray spectroscopy (EDXS) of areas containing complexes of fused deposited nanoparticles reveals the presence of both cobalt and oxygen. A representative EDXS spectrum is shown in the inset in Fig. 1(a). Consequently, the nanowires in the TEM images are interpreted as oxidized cobalt nanoparticles. The dark spots in the particles may be caused by an increased sample thickness in regions where nanoparticles are deposited on top of each other or where agglomeration leads to an increased diameter. However, it is also possible that unoxidized metallic Co inside the particles contributes to the darker areas.

Oxidation initially proceeds at the surface of the nanoparticles. It is known that metallic Co inside the particles initially resists the oxidation process, leading to the formation of Co–CoO core–shell nanoparticles.[27,28,39] While the initial oxidation leads to the formation of a <1 nm thick shell layer within several minutes, additional oxidation proceeds on a much slower time scale, on the order of several hours.[28] This suggests that the formed nanoparticles mainly consist of cobalt oxide, with regions of unoxidized metallic Co in their interior.

The two common oxidation states of cobalt are CoO [cobalt (II) oxide] and Co_3O_4 [cobalt(II,III) oxide]. Previous studies employing different synthesis methods showed that upon exposure to oxygen at room temperature, Co nanoparticles prefer the cobalt (II) oxide form.[27,39,40] In order to reveal the stoichiometry of the He droplet synthesized cobalt oxide nanoparticles, an analysis of diffractograms for selected nanoparticles is performed. The diffractograms are obtained by fast Fourier transformation (FFT) of TEM images that exhibit periodic structures corresponding to the crystal lattice. CoO has a rock salt crystal structure (cubic, $Fm\bar{3}m$), consisting of two interpenetrating fcc sublattices of Co^{2+} and O^{2-}. The lattice constant of CoO is 0.426 nm whereas the lattice constant for spinel Co_3O_4 (cubic, $Fd\bar{3}m$) is 0.808 nm.[41] An example of this approach can be seen in Fig. 2, which shows a HR-TEM image at high magnification. The inset shows a diffractogram obtained from the top most nanoparticle to the left of the inset. Diffraction spots are clearly visible and can be assigned. Note that the presented diffractogram has been corrected by employing a bandpass filter in order to improve the visibility of the diffraction spots.

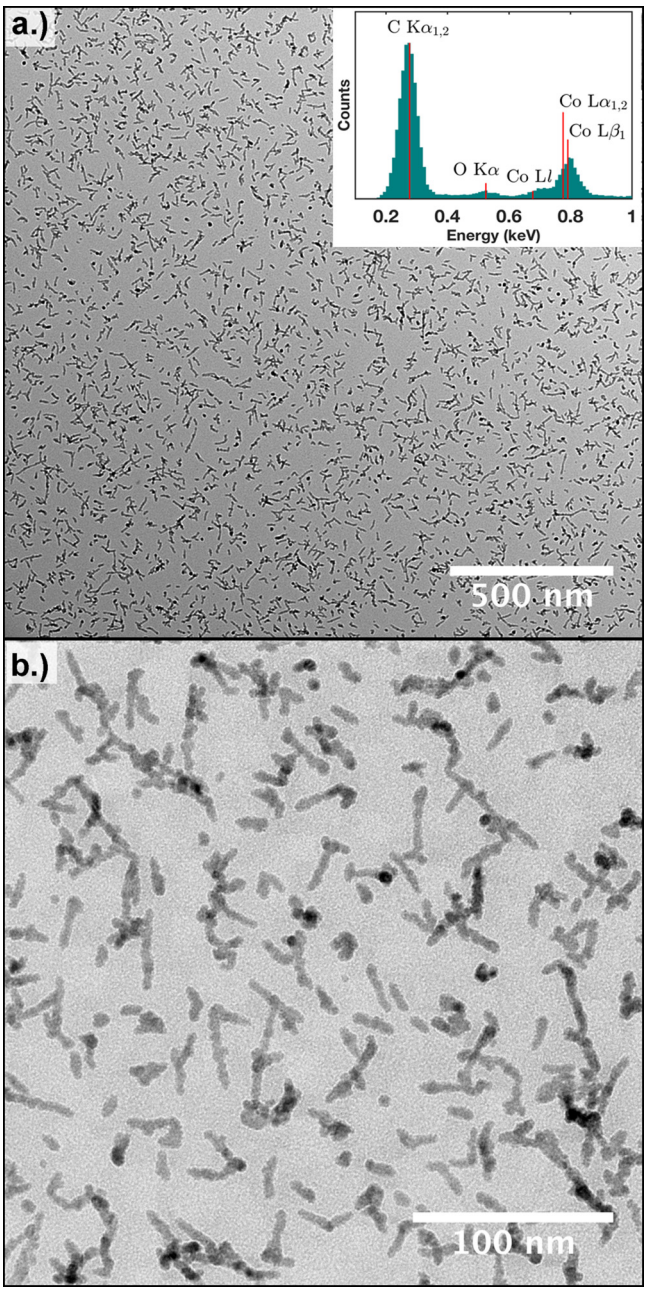

FIG. 1. Panels (a) and (b) show HR-TEM images of the produced nanoparticles at two different scales. The nanoparticles exhibit wire-like structures, some of which are fused together. The inset in panel (a) features a section of the recorded EDXS spectrum, which exhibits a carbon peak originating from the substrate, as well as cobalt and oxygen features associated with the nanoparticles.

In total, nine images with a comparable resolution as in Fig. 2, each containing a few nanoparticles, have been analyzed. Additional images can be found in the supplementary material. Among the identified diffraction spots, the most abundant lattice distances are found

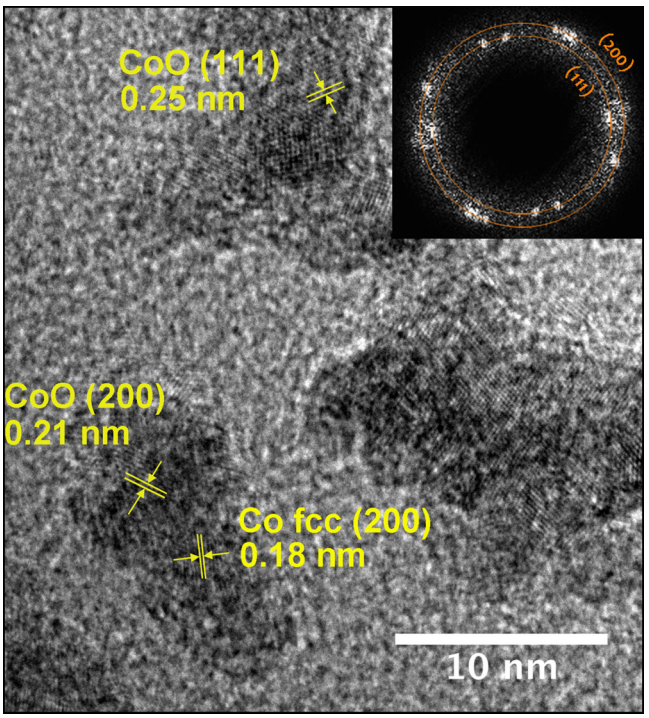

FIG. 2. Close up of a selected HR-TEM image region. Co and CoO lattices are indicated with arrows for selected particle areas. The inset shows a fast 2D Fourier transform of the area where the topmost nanoparticle is located (to the left of the inset), revealing diffraction spots associated with the (200) and (111) planes of CoO.[27]

around 0.24 nm and 0.21 nm, which match the lattice distances of the CoO (111) and (200) planes with 0.246 nm and 0.213 nm, respectively (see the supplementary material).[27] Note that these planes give rise to the two main features in x-ray powder diffraction experiments on CoO,[42] followed by less intense diffraction peaks below 0.15 nm. The uncertainty of the measurement is estimated with about 0.01 nm. Furthermore, we also find lattice distances between 0.18 nm and 0.21 nm, indicating the presence of pristine Co, which exhibits diffraction features in this range.[43] At room temperature and exposure to ambient air, it has been shown that hcp α-Co (hexagonal, $P6_3/mmc$) is preferentially formed.[44] However, the fcc phase β-Co (cubic, $Fm\bar{3}m$) exhibits prominent features in this range as well (see Table S1 in the supplementary material). We do not find any lattice distances larger than 0.25 nm, which would be clear evidence for the formation of Co_3O_4. If present, one would expect diffraction spots associated with lattice distances of 0.286 nm and 0.467 nm,[39] corresponding to the (220) and (111) planes, respectively.[27,45]

The lattice distances for selected particle areas are indicated in Fig. 2, associated with the (111) and (200) planes of CoO and the (200) plane of Co. Based on this analysis, we conclude that the nanowires consist predominantly of CoO. However, the presence of metallic Co lattices in the particles clearly shows that some particles contain regions with unoxidized Co in their interior, in agreement with previous results.[27,28]

With the structure and composition of the deposited nanoparticles determined from the TEM images and EDXS data, we proceed in the following to demonstrate the feasibility of ultrafast XUV absorption spectroscopy as a means to investigate these particles. Note that the TEM analysis employs amorphous carbon grids while the XUV absorption experiments are carried out using ultrathin Si_3N_4 substrates. However, previous experiments on metal particles synthesized using the He droplet approach showed no differences between silicon nitride[46] and carbon[26] substrates. The helium droplet source conditions (20 bar, 5.4 K), which determine the particle size and structure, and the deposition time (120 min) are identical for both employed substrates.

Figure 3 shows an XUV absorption spectrum (black) of the deposited nanoparticles on a 10 nm thick Si_3N_4 substrate. Absorption spectra are obtained by recording reference spectra without sample

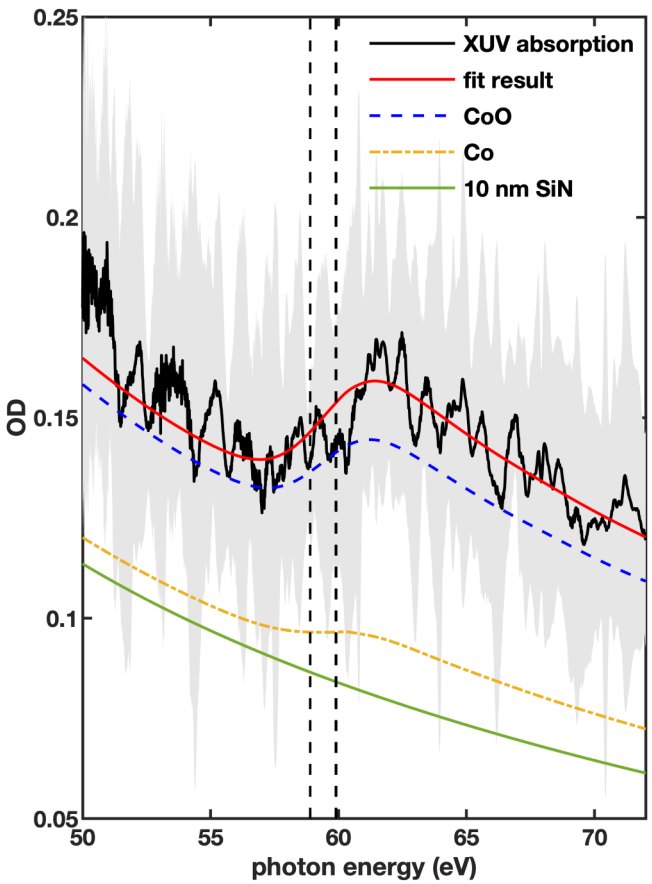

FIG. 3. XUV absorption spectrum of a sub-monolayer of nanoparticles deposited on a 10 nm thick Si_3N_4 substrate. The black spectrum is plotted together with a gray-shaded 1σ uncertainty range. The spectrum is well described by a simulation (red), consisting of a superposition of XUV absorption spectra of Co (orange), CoO (blue), and the Si_3N_4 substrate (green).[48] Note that the plotted Co and CoO components include the substrate effect as offset. The spectrum has been recorded within 6 min of total exposure time using a laboratory-based HHG source.

(I_{ref}) and spectra with sample inserted (I_{sig}) in the XUV beam and are given in units of optical density: $OD = \log(I_{ref}/I_{sig})$. The presented spectrum is derived by averaging over six static absorption spectra, followed by application of an FFT-based smoothing algorithm. The gray-shaded area in Fig. 3 corresponds to the 1σ uncertainty range of the unsmoothed signal. The Co M_2 ($3P_{1/2}$) and M_3 ($3P_{3/2}$) absorption edges are located at 58.9 eV and 59.9 eV, respectively (indicated by vertical dashed lines).[47] The corresponding increase in absorption can clearly be identified in the recorded spectrum, peaking around 62 eV. The peak height is approximately 40 mOD with respect to a background, which has been estimated by extrapolating the signal from 50 to 55 eV with an exponentially decreasing function.

The recorded XUV absorption spectrum is described by a superposition of individual Co (orange) and CoO (blue) spectra, as well as a contribution from the Si_3N_4 substrate (green). Co_3O_4 is not considered based on the results of the TEM analysis. Component spectra are taken from the online database of the Center for X-ray Optics (CXRO).[48] A least squares fit procedure is performed based on the function $OD(E) = OD_{Si}(E) + a\ OD_{CoO}(E) + b\ OD_{Co}(E)$, which includes the contributions of the three materials to the overall absorption and two free fit parameters, a and b, in order to describe the total optical density (OD) of the sample as a function of the photon energy E. $OD_{CoO}(E)$ and $OD_{Co}(E)$ are reference spectra for thin films with 4.5 nm thickness, corresponding to the estimated diameter of the nanowires. The fit result is shown as red curve in Fig. 3. Note that, for better visualization, the blue CoO and orange Co curves in Fig. 3 include the green substrate contribution as well.

The spectrum can only be described if a considerable amount of CoO is taken into account because of the broad background originating from oxygen 2s and 2p valence absorption. This gives rise to increased absorption below the M edge, a contribution that is required to describe the peak form accurately and that is absent in the metallic Co absorption spectrum. The best fit is obtained for a composition of (20 ± 7)% Co and (80 ± 9)% CoO (fit parameters $a = 0.07 \pm 0.02$, $b = 0.28 \pm 0.02$). The fit excludes data below 55 eV, which leads to a slightly better reproduction of the main peak structure. A detailed analysis of the fit suggests that as long as the Co/CoO ratio remains below ≈0.8 (45%/55%), the fit result describes the spectrum reasonably well [the variation of the root mean square (rms) error is below 3%]. While marked by substantial uncertainties, the fit result confirms that CoO is the dominant species, presumably complemented by a small contribution of metallic Co, in good agreement with conclusions from the TEM and EDXS measurements.

It is also possible to estimate the total surface coverage from the XUV spectra. Fitting the absorption spectrum by a superposition of the absorption spectra of 4.5 nm thick Co and CoO films with the above 1:4 abundance ratio, a surface coverage of (35 ± 4)% is obtained from the sum of the coefficients a and b. This value remains fairly constant for different Co/CoO ratios. To approximate the nanoparticle shapes by cylindrical rods, the value has to be multiplied by $\frac{4}{\pi}$, resulting in an estimated surface coverage between 35% and 45%, slightly larger than the (23 ± 6)% obtained from the TEM images. Note that the estimate from the XUV absorption spectra is subject to considerable uncertainties. For instance, the Si_3N_4 substrate may not exhibit a uniform 10 nm thickness as assumed, the exact three-dimensional shape of the particles is not known, and the fit model relies on data for the XUV absorption of thin filters, while nanoparticles may behave differently. Considering the uncertainties accompanying this analysis, the agreement between the surface coverage from the XUV measurements and the TEM analysis is acceptable.

The relatively low signal-to-noise ratio in the XUV absorption spectrum in Fig. 3 is a consequence of the employed apparatus, which was designed for gas-phase experiments. As a result, the time between the recording of signal and reference images was on the order of several tens of seconds. Thus, fluctuations in the stability of the HHG source, which are much faster, cannot be accounted for, causing the large noise. In future experiments, we expect that the signal can be greatly improved using more stable laser sources and a shorter period between the recording of signal and reference spectra. In particular, the noise caused by instabilities of the HHG source is less critical in a pump–probe setup where fast switching between the reference and the signal (periods with the pump laser off and on, respectively) is straightforward. The height of the main absorption peak around 62 eV of about 40 mOD will increase with surface coverage. This, however, entails the risk of particle coagulation on the substrate. Considering that recent XUV absorption experiments have shown that a change in the optical density down to 1 mOD can be detected,[49] our results suggest that the investigation of photoinduced dynamics in separated nanoparticles is likely possible with HHG based XUV transient absorption spectroscopy. Based on these estimates, photoinduced spectral changes in the investigated nanoparticles would have to be larger than about 3% in order to be detectable in a transient absorption spectroscopy experiment.

IV. CONCLUSIONS

In summary, nanowire-shaped particles are synthesized by agglomeration of Co atoms along the cores of quantum vortices inside superfluid He nanodroplets followed by deposition and oxidation on ultrathin substrates. A table-top XUV absorption spectrum recorded within minutes demonstrates that an investigation of deposited nanoparticles with a surface coverage far below a monolayer is possible with an HHG based light source, paving the way for time-resolved pump–probe experiments on these systems. The employed synthesis of nanoparticles in helium nanodroplets provides a solvent- and surfactant-free method to produce clean nanoparticles with the advantage of a very soft deposition process. The latter is crucial for a decoration of ultrathin, XUV-transparent substrates that are required for XUV absorption spectroscopy. An analysis of the deposited particles by transmission electron microscopy reveals that the synthesis method based on the deposition of metallic Co particles, which are subsequently exposed to ambient air, results in the formation of cobalt(II) oxide (CoO) nanoparticles. Both methods, transmission electron microscopy and XUV absorption spectroscopy, indicate that some particles retain an unoxidized Co core region.

Even though the XUV absorption of the deposited particles is relatively low, our results suggest that standard state-of-the-art XUV transient absorption spectroscopy setups may be used to study photoinduced dynamics in nanoparticles. Therefore, XUV absorption based spectroscopies could provide a formidable approach with

unique elemental site-specificity and unprecedented temporal resolution for the study of charge carrier dynamics[31] that underlie photocatalytic processes in transition metal oxide nanoparticles. This may be particularly interesting for an investigation of plasmon-induced charge carrier dynamics, [3,50,51] considering that the helium droplet synthesis approach easily allows for the fabrication of nanoparticles that combine plasmonic materials and transition metal oxides.[25,46] Other applications may address the dynamics in small magnetic systems, such as Co nanoparticles, similar to recent attosecond spectroscopy experiments on Ni containing thin films.[52]

ACKNOWLEDGMENTS

Support from the Austrian Science Fund (FWF) under Grant No. P30940-N36 as well as NAWI Graz and the Österreichische Forschungsgemeinschaft (ÖFG) is gratefully acknowledged. B.W.T. and O.G. are supported by the U.S. Department of Energy, Office of Science, Office of Basic Energy Sciences, Chemical Sciences, Geosciences and Biosciences Division, through Contract No. DE-AC02- 05CH11231.

DATA AVAILABILITY

The data that support the findings of this study are available from the corresponding author upon reasonable request.

REFERENCES

[1]E. Roduner, "Size matters: Why nanomaterials are different," Chem. Soc. Rev. **35**(7), 583–592 (2006).

[2]D. Wang and D. Astruc, "The recent development of efficient Earth-abundant transition-metal nanocatalysts," Chem. Soc. Rev. **46**(3), 816–854 (2017).

[3]C. Clavero, "Plasmon-induced hot-electron generation at nanoparticle/metal-oxide interfaces for photovoltaic and photocatalytic devices," Nat. Photonics **8**(2), 95–103 (2014).

[4]C.-M. Jiang, L. R. Baker, J. M. Lucas, J. Vura-Weis, A. P. Alivisatos, and S. R. Leone, "Characterization of photo-induced charge transfer and hot carrier relaxation pathways in spinel cobalt oxide (Co_3O_4)," J. Phys. Chem. C **118**(39), 22774–22784 (2014).

[5]J. Vura-Weis, C.-M. Jiang, C. Liu, H. Gao, J. M. Lucas, F. M. de Groot, P. Yang, A. P. Alivisatos, and S. R. Leone, "Femtosecond $M_{2,3}$-edge spectroscopy of transition-metal oxides: Photoinduced oxidation state change in α-Fe_2O_3," J. Phys. Chem. Lett. **4**(21), 3667–3671 (2013).

[6]L. R. Baker, C.-M. Jiang, S. T. Kelly, J. M. Lucas, J. Vura-Weis, M. K. Gilles, A. P. Alivisatos, and S. R. Leone, "Charge carrier dynamics of photoexcited Co_3O_4 in methanol: Extending high harmonic transient absorption spectroscopy to liquid environments," Nano Lett. **14**(10), 5883–5890 (2014).

[7]L. Liao, Q. Zhang, Z. Su, Z. Zhao, Y. Wang, Y. Li, X. Lu, D. Wei, G. Feng, and Q. Yu, "Efficient solar water-splitting using a nanocrystalline CoO photocatalyst," Nat. Nanotechnol. **9**(1), 69 (2014).

[8]M. Zhang, M. de Respinis, and H. Frei, "Time-resolved observations of water oxidation intermediates on a cobalt oxide nanoparticle catalyst," Nat. Chem. **6**(4), 362–367 (2014).

[9]J. Zhu, K. Kailasam, A. Fischer, and A. Thomas, "Supported cobalt oxide nanoparticles as catalyst for aerobic oxidation of alcohols in liquid phase," ACS Catal. **1**(4), 342–347 (2011).

[10]D. L. Peng, K. Sumiyama, T. J. Konno, T. Hihara, and S. Yamamuro, "Characteristic transport properties of CoO-coated monodispersive Co cluster assemblies," Phys. Rev. B **60**(3), 2093–2100 (1999).

[11]A. Boatwright, C. Feng, D. Spence, E. Latimer, C. Binns, A. M. Ellis, and S. Yang, "Helium droplets: A new route to nanoparticles," Faraday Discuss. **162**, 113–124 (2013).

[12]A. Volk, P. Thaler, M. Koch, E. Fisslthaler, W. Grogger, and W. E. Ernst, "High resolution electron microscopy of Ag-clusters in crystalline and non-crystalline morphologies grown inside superfluid helium nanodroplets," J. Chem. Phys. **138**(21), 214312 (2013).

[13]J. P. Toennies and A. F. Vilesov, "Superfluid helium droplets: A uniquely cold nanomatrix for molecules and molecular complexes," Angew. Chem. Int. Ed. **43**(20), 2622–2648 (2004).

[14]C. Callegari and W. E. Ernst, in *Handbook of High-Resolution Spectroscopy*, *Chapter: Helium Droplets as Nanocryostats for Molecular Spectroscopy—From the Vacuum Ultraviolet to the Microwave Regime*, edited by M. Quack and F. Merkt (John Wiley & Sons, Chichester, 2011), pp. 1551–1594.

[15]L. F. Gomez, E. Loginov, and A. F. Vilesov, "Traces of vortices in superfluid helium droplets," Phys. Rev. Lett. **108**(15), 155302 (2012).

[16]O. Gessner and A. F. Vilesov, "Imaging quantum vortices in superfluid helium droplets," Annu. Rev. Phys. Chem. **70**, 173–198 (2019).

[17]L. F. Gomez, K. R. Ferguson, J. P. Cryan, C. Bacellar, R. M. P. Tanyag, C. Jones, S. Schorb, D. Anielski, A. Belkacem, C. Bernando, R. Boll, J. Bozek, S. Carron, G. Chen, T. Delmas, L. Englert, W. E. Epp, B. Erk, L. Foucar *et al.*, "Shapes and vorticities of superfluid helium nanodroplets," Science **345**(6199), 906–909 (2014).

[18]P. Thaler, A. Volk, M. Ratschek, M. Koch, and W. E. Ernst, "Molecular dynamics simulation of the deposition process of cold Ag-clusters under different landing conditions," J. Chem. Phys. **140**(4), 044326 (2014).

[19]E. Latimer, D. Spence, C. Feng, A. Boatwright, A. M. Ellis, and S. Yang, "Preparation of ultrathin nanowires using superfluid helium droplets," Nano Lett. **14**(5), 2902–2906 (2014).

[20]E. Loginov, L. F. Gomez, and A. F. Vilesov, "Surface deposition and imaging of large Ag clusters formed in He droplets," J. Phys. Chem. A **115**(25), 7199–7204 (2011).

[21]P. Thaler, A. Volk, F. Lackner, J. Steurer, D. Knez, W. Grogger, F. Hofer, and W. E. Ernst, "Formation of bimetallic core-shell nanowires along vortices in superfluid He nanodroplets," Phys. Rev. B **90**(15), 155442 (2014).

[22]A. Volk, P. Thaler, D. Knez, A. W. Hauser, J. Steurer, W. Grogger, F. Hofer, and W. E. Ernst, "The impact of doping rates on the morphologies of silver and gold nanowires grown in helium nanodroplets," Phys. Chem. Chem. Phys. **18**(3), 1451–1459 (2016).

[23]A. Volk, D. Knez, P. Thaler, A. W. Hauser, W. Grogger, F. Hofer, and W. E. Ernst, "Thermal instabilities and Rayleigh breakup of ultrathin silver nanowires grown in helium nanodroplets," Phys. Chem. Chem. Phys. **17**(38), 24570–24575 (2015).

[24]M. Schnedlitz, M. Lasserus, D. Knez, A. W. Hauser, F. Hofer, and W. E. Ernst, "Thermally induced breakup of metallic nanowires: Experiment and theory," Phys. Chem. Chem. Phys. **19**(14), 9402–9408 (2017).

[25]M. Lasserus, D. Knez, M. Schnedlitz, W. Hauser, A. Hofer, F. E, and W. Ernst, "On the passivation of iron particles at the nanoscale," Nanoscale Adv. **1**(6), 2276–2283 (2019).

[26]M. Schnedlitz, M. Lasserus, R. Meyer, D. Knez, F. Hofer, W. E. Ernst, and A. W. Hauser, "Stability of core–shell nanoparticles for catalysis at elevated temperatures: Structural inversion in the Ni–Au system observed at atomic resolution," Chem. Mater. **30**(3), 1113–1120 (2018).

[27]D.-H. Ha, L. M. Moreau, S. Honrao, R. G. Hennig, and R. D. Robinson, "The oxidation of cobalt nanoparticles into Kirkendall-hollowed CoO and Co_3O_4: The diffusion mechanisms and atomic structural transformations," J. Phys. Chem. C **117**(27), 14303–14312 (2013).

[28]S. Jia, C.-H. Hsia, and D. H. Son, "In situ study of room-temperature oxidation kinetics of colloidal Co nanocrystals investigated by Faraday rotation measurement," J. Phys. Chem. C **115**(1), 92–96 (2010).
[29]A. Schiffmann, D. Knez, F. Lackner, M. Lasserus, R. Messner, M. Schnedlitz, G. Kothleitner, F. Hofer, and W. E. Ernst, "Ultra-thin h-BN substrates for nanoscale plasmon spectroscopy," J. Appl. Phys. **125**(2), 023104 (2019).
[30]P. M. Kraus, M. Zürch, S. K. Cushing, D. M. Neumark, and S. R. Leone, "The ultrafast x-ray spectroscopic revolution in chemical dynamics," Nat. Rev. Chem. **2**(6), 82–94 (2018).
[31]R. Geneaux, H. J. Marroux, A. Guggenmos, D. M. Neumark, and S. R. Leone, "Transient absorption spectroscopy using high harmonic generation: A review of ultrafast x-ray dynamics in molecules and solids," Philos. Trans. R. Soc. A **377**(2145), 20170463 (2019).
[32]M. E. Vaida, B. M. Marsh, and S. R. Leone, "Nonmetal to metal transition and ultrafast charge carrier dynamics of Zn clusters on p-Si(100) by fs-XUV photoemission spectroscopy," Nano Lett. **18**(7), 4107–4114 (2018).
[33]P. Thaler, A. Volk, D. Knez, F. Lackner, G. Haberfehlner, J. Steurer, M. Schnedlitz, and W. E. Ernst, "Synthesis of nanoparticles in helium droplets—A characterization comparing mass-spectra and electron microscopy data," J. Chem. Phys. **143**(13), 134201 (2015).
[34]L. F. Gomez, E. Loginov, R. Sliter, and A. F. Vilesov, "Sizes of large He droplets," J. Chem. Phys. **135**(15), 154201 (2011).
[35]E. Loginov, L. F. Gomez, N. Chiang, A. Halder, N. Guggemos, V. V. Kresin, and A. F. Vilesov, "Photoabsorption of Ag_N ($N \sim 6$–6000) nanoclusters formed in helium droplets: Transition from compact to multicenter aggregation," Phys. Rev. Lett. **106**(23), 233401 (2011).
[36]M.-F. Lin, A. N. Pfeiffer, D. M. Neumark, S. R. Leone, and O. Gessner, "Strong-field induced XUV transmission and multiplet splitting in $4d^{-1}6p$ core-excited Xe studied by femtosecond XUV transient absorption spectroscopy," J. Chem. Phys. **137**(24), 244305 (2012).
[37]B. W. Toulson, M. Borgwardt, H. Wang, F. Lackner, A. S. Chatterley, C. D. Pemmaraju, D. M. Neumark, S. R. Leone, D. Prendergast, and O. Gessner, "Probing ultrafast C–Br bond fission in the UV photochemistry of bromoform with core-to-valence transient absorption spectroscopy," Struct. Dyn. **6**(5), 054304 (2019).
[38]J. Schindelin, I. Arganda-Carreras, E. Frise, V. Kaynig, M. Longair, T. Pietzsch, S. Preibisch, C. Rueden, S. Saalfeld, B. Schmid, J.-Y. Tinevez, D. J. White, V. Hartenstein, K. Eliceiri, P. Tomancak, and A. Cardona, "Fiji: An open-source platform for biological-image analysis," Nat. Methods **9**(7), 676–682 (2012).
[39]J. B. Tracy, D. N. Weiss, D. P. Dinega, and M. G. Bawendi, "Exchange biasing and magnetic properties of partially and fully oxidized colloidal cobalt nanoparticles," Phys. Rev. B **72**(6), 064404 (2005).
[40]P. Bazylewski, D. W. Boukhvalov, A. I. Kukharenko, E. Z. Kurmaev, A. Hunt, A. Moewes, Y. H. Lee, S. O. Cholakh, and G. S. Chang, "The characterization of Co-nanoparticles supported on graphene," RSC Adv. **5**(92), 75600–75606 (2015).
[41]J. Wang, "Low energy electron diffraction studies of transition metal oxide surfaces and films," Ph.D. thesis (Martin-Luther-Universität Halle-Wittenberg, 2005).
[42]M. Ghosh, E. V. Sampathkumaran, and C. N. R. Rao, "Synthesis and magnetic properties of CoO nanoparticles," Chem. Mater. **17**(9), 2348–2352 (2005).
[43]L. Meziane, C. Salzemann, C. Aubert, H. Gérard, C. Petit, and M. Petit, "Hcp cobalt nanocrystals with high magnetic anisotropy prepared by easy one-pot synthesis," Nanoscale **8**(44), 18640–18645 (2016).
[44]V. A. de la Peña O'Shea, I. d. P. R. Moreira, A. Roldán, and F. Illas, "Electronic and magnetic structure of bulk cobalt: The α, β, and ϵ-phases from density functional theory calculations," J. Chem. Phys. **133**(2), 024701 (2010).
[45]C. Y. Ma, Z. Mu, J. J. Li, Y. G. Jin, J. Cheng, G. Q. Lu, Z. P. Hao, and S. Z. Qiao, "Mesoporous Co_3O_4 and Au/Co_3O_4 catalysts for low-temperature oxidation of trace ethylene," J. Am. Chem. Soc. **132**(8), 2608–2613 (2010).
[46]M. Schnedlitz, R. Fernandez-Perea, D. Knez, M. Lasserus, A. Schiffmann, F. Hofer, A. W. Hauser, M. P. de Lara-Castells, and W. E. Ernst, "Effects of the core location on the structural stability of Ni–Au core–shell nanoparticles," J. Phys. Chem. C **123**(32), 20037–20043 (2019).
[47]A. C. Thompson and D. Vaughan, *X-Ray Data Booklet*, 3rd ed. (Lawrence Berkeley National Library, 2009).
[48]B. L. Henke, E. M. Gullikson, and J. C. Davis, "X-ray interactions photoabsorption, scattering, transmission, and reflection at $E = 50$–30,000 eV, $Z = 1$–92," At. Data Nucl. Data Tables **54** (2), 181–342 (1993).
[49]Z. Wei, L. Tian, J. Li, Y. Lu, M. Yang, and Z.-H. Loh, "Tracking ultrafast bond dissociation dynamics at 0.1 Å resolution by femtosecond extreme ultraviolet absorption spectroscopy," J. Phys. Chem. Lett. **9**(19), 5742–5747 (2018).
[50]A. Naldoni, F. Riboni, U. Guler, A. Boltasseva, V. M. Shalaev, and A. V. Kildishev, "Solar-powered plasmon-enhanced heterogeneous catalysis," Nanophotonics **5**(1), 112–133 (2016).
[51]M. L. Brongersma, N. J. Halas, and P. Nordlander, "Plasmon-induced hot carrier science and technology," Nat. Nanotechnol. **10**(1), 25–34 (2015).
[52]F. Siegrist, J. A. Gessner, M. Ossiander, C. Denker, Y.-P. Chang, M. C. Schröder, A. Guggenmos, Y. Cui, J. Walowski, U. Martens, J. K. Dewhurst, U. Kleineberg, M. Münzenberg, S. Sharma, and M. Schultze, "Light-wave dynamic control of magnetism," Nature **571**(7764), 240–244 (2019).